Journal of Molecular Catalysis A: Chemical 315 (2010) 187–196

Contents lists available at ScienceDirect

Journal of Molecular Catalysis A: Chemical

journal homepage: www.elsevier.com/locate/molcata

# Investigation the active site of methane dissociation on Ni-based catalysts: A first-principles analysis

Bin Xing[a], Xian-Yong Pang[a], Gui-Chang Wang[b,*], Zhen-Feng Shang[b,*]

[a] College of Chemistry and Chemical Engineering, Taiyuan University of Technology, Taiyuan 030024, PR China
[b] Department of Chemistry, Nankai University, Tianjin 300071, PR China

ARTICLE INFO

*Article history:*
Received 10 June 2009
Received in revised form
17 September 2009
Accepted 17 September 2009
Available online 24 September 2009

*Keywords:*
Methane dissociation
Ni surface
Active site
Density functional theory calculation
Slab model

ABSTRACT

The adsorption and dissociation of $CH_4$ on clean Ni(1 0 0), oxygen atom pre-adsorbed Ni(1 0 0) and NiO(1 0 0) surfaces have been studied using density functional theory calculations with the periodic slab model. The activation barrier for methane dissociation on clean Ni(1 0 0) is much lower than that on the oxygen atom pre-adsorbed Ni(1 0 0) and NiO(1 0 0) surface. Thus the active site for methane dissociation is the metallic Ni instead of the oxidized Ni. Moreover, the decomposition of activation barrier has been performed. The result further explains how the existence of oxygen atom increases the barrier. Though the pre-adsorbed oxygen atom decreases the interaction between $CH_3$ and H in the transition state, it greatly decreases the interaction of $CH_3$ and H with substrate. So the overall result is that the oxygen atom inhibits the dissociation of methane on Ni surface. Importantly, it was found that a three-center bond formed in the transition state when oxygen atom acts as a spectator, which leading to a smaller energy barrier for the reaction of $CH_4 + O \rightarrow CH_3 + H + O$ than that of $CH_4 + O \rightarrow CH_3 + OH$.



## 1. Introduction

The dissociative adsorption of methane on transition metal catalyst to form surface-bound methyl and hydrogen is an important step in the steam reforming process which converts natural gas to a mixture of carbon monoxide and hydrogen [1,2]. In particular, the methyl radical has been believed to be a key intermediate because it is the nascent product of the $CH_4$ dissociation. Therefore, the study of the chemisorption of methyl on the nickel surface could provide important information. In addition, metallic nickel is the efficient catalyst. So the dissociative adsorption of $CH_4$ has led to a number of experimental and theoretical studies [3–18].

Experimentally, direct measurements of thermal sticking coefficient have been carried out for $CH_4$ on Ni(1 0 0) [4,5]. The energy barrier for the dissociation reaction was estimated to be 0.28 eV [4] and 0.54 eV [5]. Nielsen et al. [6] performed reliable measurement of the activation energy barrier for $CH_4$ dissociative adsorption on Ni(1 0 0) surface gave a value of 0.61 eV, much lower than that on Ni(1 1 1) surface (0.77 eV) [7]. Several studies indicate that the dissociation of $CH_4$ on Ni(1 0 0) is a direct process that can be activated by both incident kinetic energy normal to the surface and thermal vibrational energy of the incident $CH_4$ [1,10–12]. Hu and Ruckenstein [13] studied the partial oxidation of methane and found that the metallic Ni is more active than the oxidized Ni for $CH_4$ activation. Furthermore, they also performed experiment with the deuterium–methane pulses method to study the dissociation of methane on Ni [14]. The experimental results showed that $CH_4$ can easily dissociate into $CH_x$ and H on a metallic Ni catalyst, whereas such a dissociation reaction cannot take place on the catalyst in the oxidized state [14]. Campbell et al. [15] reported that the reaction probability of methane on NiO films is significantly lower than that on clean Ni(1 0 0) surface.

Recently, Beck et al. [9] report quantum state-resolved studies of vibrationally excited $CH_4$ reacting on the Ni(1 0 0) surface. Their results clearly exclude the possibility of statistical models correctly describing the mechanism of this process and attest to the importance of full-dimensional calculations of the reaction dynamics. So, despite many experimental works have been performed to an understanding of the dissociative chemisorption of methane on Ni surface, the theoretical analysis is still valuable to further understand such a complex dynamical reaction [1,3,8,16–18]. Bengaard et al. [8] performed the self-consistent density functional theory (DFT) calculations and obtained an activation barrier of 1.17 eV. Burghgraef et al. [16] have found that the activation barrier was 0.42 eV for a single Ni atom, 2.25 eV for the $Ni_7$-cluster and 1.25 eV for the $Ni_{13}$-cluster. Swang et al. [17] studied the dissociative adsorption of $CH_4$ on the Ni(1 0 0) surface at the ab initio complete active space self-consistent field (CASSCF) level. They found the energy barrier was in the range of $0.69 \pm 0.04$ eV using a cluster model. Moreover, although many researches have focused on such typical surface reaction, some questions are still

* Corresponding author. Tel.: +86 22 23503824; fax: +86 22 23502458.
*E-mail addresses:* wangguichang@nankai.edu.cn (G.-C. Wang), zfshang@nankai.edu.cn (Z.-F. Shang).

1381-1169/$ – see front matter © 2009 Elsevier B.V. All rights reserved.
doi:10.1016/j.molcata.2009.09.010

unclear. For example, what is the active site for the methane dissociation on Ni-based catalysts, metallic Ni or oxidized Ni? How is the dissociation of $CH_4$ affected by the pre-adsorbed oxygen atoms?

In this study, the following schemes were used to study the active site: the clean Ni(1 0 0) surface was used to simulate the metallic Ni; the oxygen atom pre-adsorbed Ni(1 0 0) (O/Ni(1 0 0)) and the NiO(1 0 0) surfaces were used to simulate the oxidized Ni. For the situations of oxygen atom pre-adsorbed Ni(1 0 0) surfaces, the influence of different oxygen atom coverage ($\theta_O$ = 1/2, 1/4, 1/6 and 1/9 monolayer (ML)) has also been considered. By the comparison of the activation barrier on various catalysts, we intended to explore the possible active site for the methane dissociation. Our paper is organized as follows. In Section 2, we introduce the details of calculation methods and the models. The calculated adsorption energies and activation barriers are given in Section 3. These results are compared with previous works to examine the accuracy of our method.

## 2. Calculation methods and models

To study the energy and structure details of $CH_4$ dissociation on Ni surface, the periodic, self-consistent DFT calculation was performed by using the Vienna ab initio simulation package (VASP) [19–21]. The electronic structures were calculated using DFT within the generalized gradient approximation (GGA-PW91) [22–24]. The project-augment wave (PAW) [23,24] scheme was used to describe the inner cores, and the electronic states were expended in a plane wave basis with kinetic cut-off energy of 350 eV. The climbing-nudged elastic band (cNEB) method was employed to locate the transition state [25–27]. Lastly, the frequency analysis was performed to confirm the transition state. Vibrational frequencies are calculated by numerical differentiation of the forces using a second order finite difference approach with a step size of 0.015 Å. Based on the calculated frequency results, the zero point energy (ZPE) correction has been taken into account. It was found that the ZPE corrections for different system are nearly identical (~0.20 eV). Thus we do not list the energy data with the ZPE correction. The surfaces were modeled by a periodic slab containing four atomic layers with a full relaxation of the uppermost two layers (Fig. 1). In our calculations, three different super-cells with $p(2 \times 2)$, $(3 \times 2)$ and $(3 \times 3)$ were chosen to represent different coverage of pre-adsorbed oxygen atom. Specially, the $p(3 \times 3)$ slab model was built with three atomic layers, while the first layer was allowed to relax. For the different systems in the calculations, the Monkhorst–Pack meshes of $4 \times 4 \times 1$, $4 \times 6 \times 1$ and $3 \times 3 \times 1$ special $k$-point sampling in the surface Brillouin zone [28] were used for the $(2 \times 2)$, $(3 \times 2)$ and $(3 \times 3)$ system, respectively. A large $k$-point of $9 \times 9 \times 1$ was chosen during the calculation of electronic structures for the accurate results. All the calculations considered magnetic properties of Ni atom based on the spin-polarization method. The calculated lattice constant of metallic Ni is 3.53 Å, which is close to the experimental data (3.52 Å) and as well as other theoretical results (3.54 Å) [29]. The calculated magnetic moment of fcc Ni at the equilibrium lattice constant is $0.629\mu_B$, which agrees well with the theoretical value of $0.626\mu_B$ [30] and the experimental value of $0.606\mu_B$ [31]. The lattice constant of 4.18 Å is used for NiO(1 0 0) The adsorption energy ($E_{ads}$) and the activation barrier ($E_a$) were calculated as the two formulas: $E_{ads} = E_{A/M} - E_A - E_M$ and $E_a = E_{TS} - E_{IS}$, respectively. Here, $E_A$, $E_M$, $E_{A/M}$, $E_{TS}$ and $E_{IS}$ mean the calculated energy of adsorbates, substrate, adsorption system, transition state and initial state, respectively.

Different calculation parameters such as number of layers and $k$-point sampling were considered to select the most reasonable ones. Different number of layers can affect calculated adsorption energy. $CH_3$ adsorbed on the different models (four-layers and six-layers) were studied, and the energy difference was found to be less than 0.02 eV. So the model of four-layers is more reasonable. Similarly, for the $k$-point sampling used in the calculation, two sets of $k$-point of $5 \times 5 \times 1$ and $6 \times 6 \times 1$ have been compared with $4 \times 4 \times 1$. The results indicated that adsorption energy difference is 0.07 and 0.02 eV respective to the $4 \times 4 \times 1$. So $4 \times 4 \times 1$ is used in this calculation.

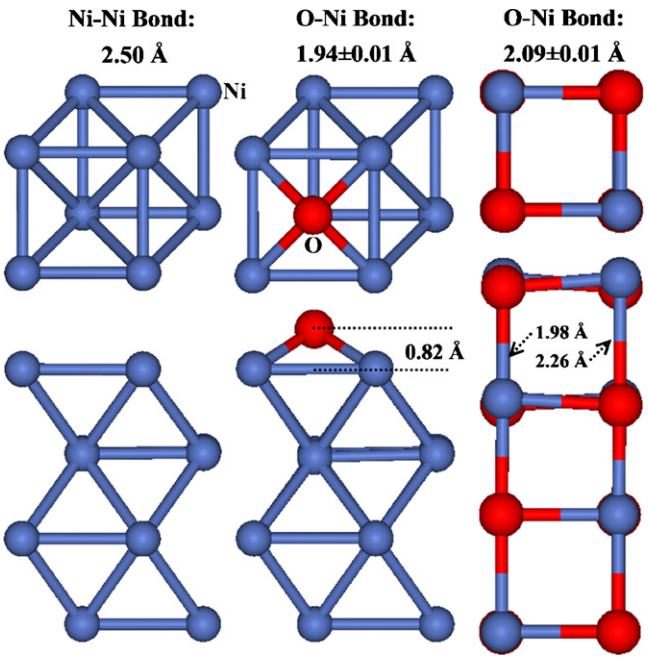


**Fig. 1.** Top view and side view of optimized bare Ni(1 0 0), O/Ni(1 0 0) and NiO(1 0 0) surface models.

## 3. Results and discussion

### 3.1. Adsorption properties of possible species

We mainly studied the first dissociation step of $CH_4$, so the possible adsorption species are $CH_4$, $CH_3$ and H. Specially for the O/Ni(1 0 0) surface with higher oxygen atom coverage, the H fragment tends to form hydroxyl with pre-adsorbed oxygen atom, thus the adsorption of hydroxyl has also been calculated. The corresponding energies and geometry parameters are listed in Tables 1–4.

#### 3.1.1. $CH_4$

To study the dissociation of $CH_4$ on clean Ni(1 0 0) surface, O/Ni(1 0 0) surfaces and NiO(1 0 0) surface, the stable adsorption site for $CH_4$ was necessary to be confirmed, from which the reaction pathway could be calculated.

**Table 1**
Adsorption energies and geometries of methane on different surfaces.[a]

| Surfaces | $E_{ads}$ (eV) | $d_{C-Ni}$ (Å) | $d_{C-H}$ (Å) |
|---|---|---|---|
| Ni(1 0 0) | 0.10 | 2.73 | 1.10 (2), 1.11 (2) |
| O/Ni(1 0 0) | | | |
| 1. $\theta_O$ = 1/2 ML | 0.09 | 3.44 | 1.09, 1.10 (3) |
| 2. $\theta_O$ = 1/4 ML | 0.03 | 3.30 | 1.10 (4) |
| 3. $\theta_O$ = 1/6 ML | 0.04 | 3.31 | 1.10 (4) |
| 4. $\theta_O$ = 1/9 ML | 0.10 | 3.20 | 1.10 (3), 1.11 |
| NiO(1 0 0) | −0.06 | 3.56 | 1.10 (4) |

[a] $d_{C-Ni}$ denotes the shortest C–Ni distances, and $d_{C-H}$ denote the lengths of C–H bonds in $CH_4$ species.

**Table 2**
Adsorption energies and geometries of methyl on different surfaces.[a].

| Sites | $E_{ads}$ (eV) | $d_{C-Ni}$ (Å) | $d_{C-H}$ (Å) |
|---|---|---|---|
| Ni(1 0 0) | | | |
| 1. Hollow | −1.93 | 2.03 | 1.11, 1.12 (2) |
| 2. Ni-Top | −1.94 | 2.03 | 1.11 (2), 1.15 |
| 3. Bridge | −1.97 | 2.01 | 1.10, 1.11, 1.15 |
| O/Ni(1 0 0) | | | |
| $\theta_O$ = 1/2 ML | | | |
| 1. Ni-Top | −1.10 | 1.99 | 1.09, 1.10 (2) |
| $\theta_O$ = 1/4 ML | | | |
| 1. Ni-Top | −1.41 | 1.96 | 1.10 (3) |
| 2. Bridge | −1.53 | 2.03 | 1.10, 1.11 (2) |
| $\theta_O$ = 1/6 ML | | | |
| 1. Ni-Top | −1.81 | 1.95 | 1.10 (3) |
| $\theta_O$ = 1/9 ML | | | |
| 1. Ni-Top | −1.84 | 1.95 | 1.10 (3) |
| NiO(1 0 0) | | | |
| 1. Ni-Top | −1.71 | 1.91 | 1.10 (3) |
| 2. Bridge | −1.60 | 1.93 | 1.10 (3) |
| 3. Hollow | −1.47 | 1.93 | 1.10 (3) |
| 4. O-top | 0.09 | 2.10 | 1.09 (3) |

[a] $d_{C-Ni}$ denotes the shortest C–Ni distances, and $d_{C-H}$ denote the lengths of C–H bonds in $CH_3$ species.

**Table 3**
Adsorption energies and geometries of H or OH on different surfaces.

| Site | $E_{ads}$ (eV) | $d_{H-Ni(O)}$ (Å) |
|---|---|---|
| Ni(1 0 0) | | |
| 1. Hollow | −2.89 | 1.80 |
| 2. Bridge | −2.77 | 1.61 |
| 3. Ni-Top | −2.28 | 1.47 |
| O/Ni(1 0 0) ($\theta_O$ = 1/4 ML) | | |
| 1. Hollow[a] | −3.71 | 0.98 |
| 2. Bridge[a] | −3.70 | 0.98 |
| 3. Ni-Top | −2.16 | 1.51 |
| NiO(1 0 0) | | |
| 1. O-top | −2.47 | 0.98 |
| 2. Ni-Top | −1.97 | 1.45 |
| 3. Bridge | −1.81 | 1.44 |
| 4. Hollow | −1.75 | 1.51 |

$d_{H-Ni(O)}$ denotes the shortest distance between H atom and surface Ni atom or the bond length of hydroxyl that form only on O/Ni and at O-top site of NiO surface.
[a] Adsorption species is hydroxyl.

**Table 4**
Adsorption energies and geometries of the most stable co-adsorption site on different surfaces.

| | $E_{ads}$ (eV) | $d_{C-Ni}$ (Å) | $d_{C-H}$ (Å) |
|---|---|---|---|
| Ni(1 0 0) | −4.60 | 2.04 | 2.72 |
| O/Ni(1 0 0) | | | |
| 1. $\theta_O$ = 1/2 ML | −4.24 | 1.99 | 2.30 |
| 2. $\theta_O$ = 1/4 ML | −4.22 | 2.02 | 4.01 |
| 3. $\theta_O$ = 1/6 ML | | | |
| $CH_3$ + OH | −4.41 | 1.98 | 4.25 |
| $CH_3$ + H | −4.27 | 2.05 | 3.04 |
| 4. $\theta_O$ = 1/9 ML | | | |
| $CH_3$ + OH | −4.47 | 1.98 | 4.25 |
| $CH_3$ + H | −4.38 | 2.03 | 2.85 |
| NiO(1 0 0) | −4.85 | 1.96 | 2.24 |

$d_{C-H}$ here denotes the distance between C atom of $CH_3$ group and the dissociated H atom from $CH_4$. $E_{ads} = E_{(CH_3+H/OH)/M} - E_{CH_3} - E_{H/OH} - E_M$.

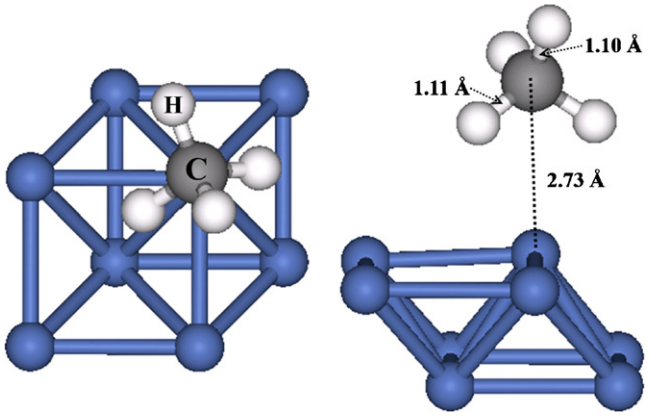


**Fig. 2.** Top view and side view of optimized $CH_4$ adsorption on clean Ni(1 0 0) surface.

The adsorption of methane on Ni(1 0 0) has been studied at the top, bridge and hollow sites. The corresponding adsorption energies are 0.10, 0.12 and 0.15 eV. The adsorption energy at top site is little smaller than other research results (±0.05 eV) [1,3]. The possible reason may be the different parameters such as *k*-points used. The distance between C atom and the surface Ni atom is 2.73 Å. Thus the physisorption of $CH_4$ on Ni(1 0 0) is evident. The optimized structure of $CH_4$ adsorption on clean Ni(1 0 0) surface at top site is shown in Fig. 2.

Before the calculating of $CH_4$ adsorption on the O/Ni(1 0 0) surface, the adsorption site for oxygen atom needed to be identified. The calculated result showed that the oxygen atom was inclined to adsorb at the four-hold hollow site, which is consistent with the results of other studies [32–35]. The calculated adsorption energy of atomic oxygen at four-hold hollow site was −6.28 eV, which is about 0.80 eV larger than that of bridge site. Goursot et al. [34] used spin-polarized linear combinations of Gaussian-type orbital-model core potential-local spin density (LCGTO-MCP-LSD) computations to study the adsorption of oxygen atom on Ni(1 0 0) surface, the adsorption energy is −6.70 eV with oxygen atom at the four-hold hollow site, which is only 0.40 eV lower than that at bridge site. Siegbahn and Wahlgren [35] have found that the most stable adsorption site for the oxygen atom is four-hold hollow site with calculated adsorption energy of −5.64 eV. Then the adsorption of $CH_4$ on the O/Ni(1 0 0) surface with different oxygen atom coverage ($\theta_O$ = 1/2, 1/4, 1/6 and 1/9 ML) was studied. The calculated adsorption energies are 0.09, 0.03, 0.04 and 0.10 eV, and the shortest distances between C atom and surface Ni atom are 3.44, 3.30, 3.31 and 3.20 Å.

For the NiO(1 0 0) surface, the adsorption energy of $CH_4$ is −0.06 eV, and the shortest distance between C atom and surface Ni atom is 3.56 Å, which is in agreement with the result calculated by Hwang and Mebel [18], in which they found that the $CH_4$ molecule can be attached without a barrier to the Ni atom of NiO.

### 3.1.2. $CH_3$

Since $CH_3$ species is the first-step product of $CH_4$ dissociation, the study of the chemisorption of $CH_3$ is important. Various potential adsorption sites for $CH_3$ on different surfaces were considered.

For clean Ni(1 0 0) surface, the most stable site for $CH_3$ species was found to be the bridge site with adsorption energy of −1.97 eV. This result is in accordance with recent theoretical calculation results obtained by Lai et al. [3] (−2.24 eV), Zhu et al. [1] (−1.98 eV) and the semi-empirical result reported by Wonchoba and Truhlar [36] (−1.86 eV). But our result is different from previous theoretical predictions by Siegbahn and Panas [37] and Upton [38] who

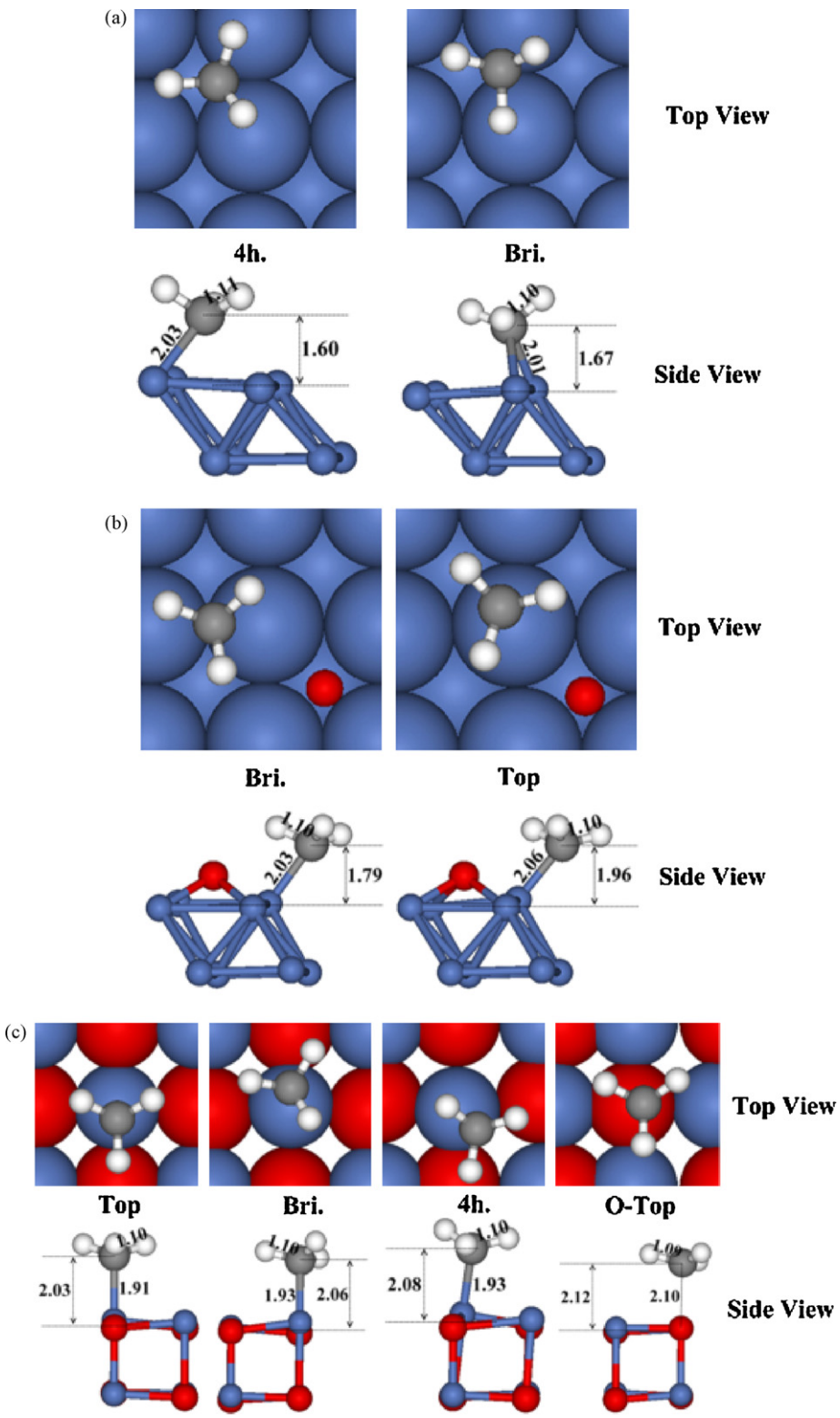


**Fig. 3.** Top view and side view with geometry parameters of $CH_3$ group adsorbed at different sites on the different surface. The illustrations corresponding to clean Ni(1 0 0), O/Ni(1 0 0) with $\theta_O$ = 1/4 ML and NiO(1 0 0) surfaces. The dark grey spheres represent Ni atoms; the light grey spheres represent C atoms; the dark spheres represent O atom; the white spheres represent H atoms. Bond lengths are in Å.

found that hollow site was the most stable site for $CH_3$. Besides the bridge site, the other two sites (top and four-hold hollow) were also investigated. The calculated adsorption energies were −1.94 and −1.93 eV. The optimized structures are shown in Fig. 3a. Since the $CH_3$ species moves to the bridge site from its initial top site, so we do not show such structure in Fig. 3a.

The adsorption of $CH_3$ on O/Ni(1 0 0) surface at different sites with $\theta_O$ = 1/4 ML was also investigated. The adsorption energies were found be −1.41 and −1.53 eV for the top and bridge site, respectively. The geometry structures of these two adsorption sites are illustrated in Fig. 3b. As a comparison, the adsorption of $CH_3$ at Ni-top site on the other O/Ni(1 0 0) surfaces ($\theta_O$ = 1/2, 1/6 and

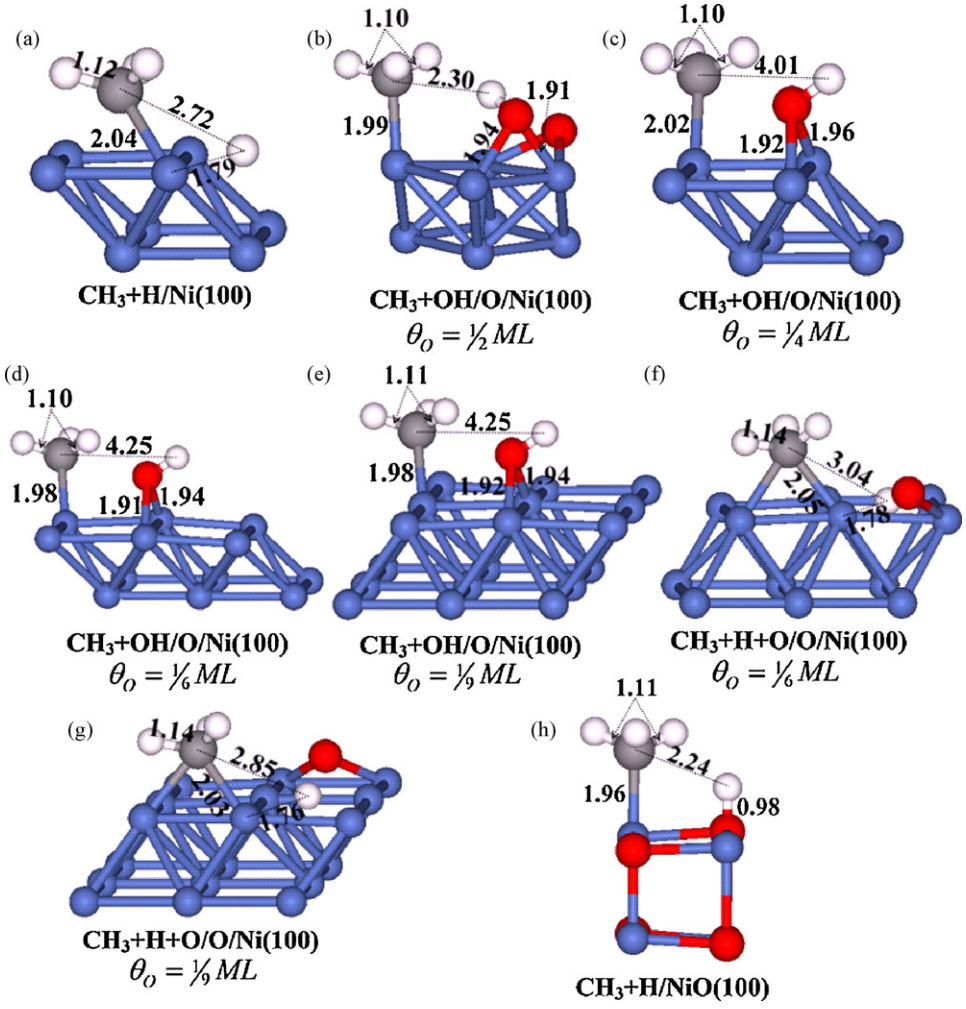


**Fig. 4.** Side view of the most stable co-adsorption site on the different surfaces. The distances are in Å.

1/9 ML) was also calculated. The corresponding energies are −1.10, −1.81 and −1.84 eV.

For the NiO(1 0 0) surface, four different adsorption sites for $CH_3$, including Ni-top, bridge, four-hold hollow and O-top site were studied. The calculated adsorption energies are −1.71, −1.60, −1.47 and 0.09 eV. The detailed geometry parameters are shown in Fig. 3c and Table 2. For $CH_3$ adsorbed at O-top site, there is no formation of new bond after optimization and the adsorption energy is only 0.09 eV. So the adsorption type is physisorption.

### 3.1.3. H/OH

The adsorption properties of H atom were also calculated at different sites on different surfaces. The H atom favors four-hold hollow site on clean Ni(1 0 0) surface. The adsorption energy of H atom at four-hold hollow was calculated to be −2.89 eV, which is 0.12 eV larger than that of bridge site and 0.61 eV lower than that of Ni-top site. This result is in agreement with the energy of −2.79 eV obtained by Zhu et al. [1] and experimental value of −2.74 eV obtained by Christmann et al. [39]. And for the O/Ni(1 0 0) surface, a typical surface ($\theta_O$ = 1/4 ML) was used to investigate the adsorption of H atom. Considering that H atom may form hydroxyl with pre-adsorbed oxygen atom, two different sites for hydroxyl (four-hold hollow site and bridge site) and Ni-top site for H atom were investigated. The adsorption energy for hydroxyl at the four-hold hollow site was calculated to be −3.71 eV, which is only 0.01 eV larger than that at bridge site. The adsorption energy of H atom at Ni-top site was calculated to be −2.16 eV. For the adsorption of H atom on NiO(1 0 0) surface, the four different possible sites including O-top, Ni-top, bridge and four-hold hollow site were studied. The corresponding adsorption energies are −2.47, −1.97, −1.81 and −1.75 eV. The details of geometry parameters are listed in Table 3.

## 3.2. Reaction energy of $CH_4$ dissociation on different catalysts

Since the NEB method depends largely on the structures of reactant and product, it is necessary to determine the most stable form of the initial state (IS) and the final state (FS). The IS is the adsorption of $CH_4$, which has already been studied in Section 3.1. The reaction mechanism is the direct dissociation of $CH_4$ on Ni(1 0 0) surface and NiO(1 0 0) surface, so the FS is $CH_3$ + H, namely, $CH_4(a) \rightarrow CH_3(a) + H(a)$. The reaction mechanisms on O/Ni(1 0 0) surfaces vary according to the different coverage of pre-adsorbed oxygen atom: for the higher coverage ($\theta_O$ = 1/2 and 1/4 ML) the dissociated H atom tends to form hydroxyl with the pre-adsorbed oxygen atom, so the FS is $CH_3$ + OH; but for the lower coverage ($\theta_O$ = 1/6 and 1/9 ML) the FS of $CH_3$ + OH or $CH_3$ + H + O are possible. In fact, the FS form of $CH_3$ + H + O has also been studied, and it was found that the final state is $CH_3$ + OH after optimization.

### 3.2.1. Ni(1 0 0)

Four different combinations of adsorption configurations for $CH_3$ and H were chosen to find a more stable FS, including $CH_3$(bri.) + H(bri.), $CH_3$(top) + H(bri.), $CH_3$(bri.) + H(4h.) and $CH_3$(4h.) + H(4h.). The most stable system was found to

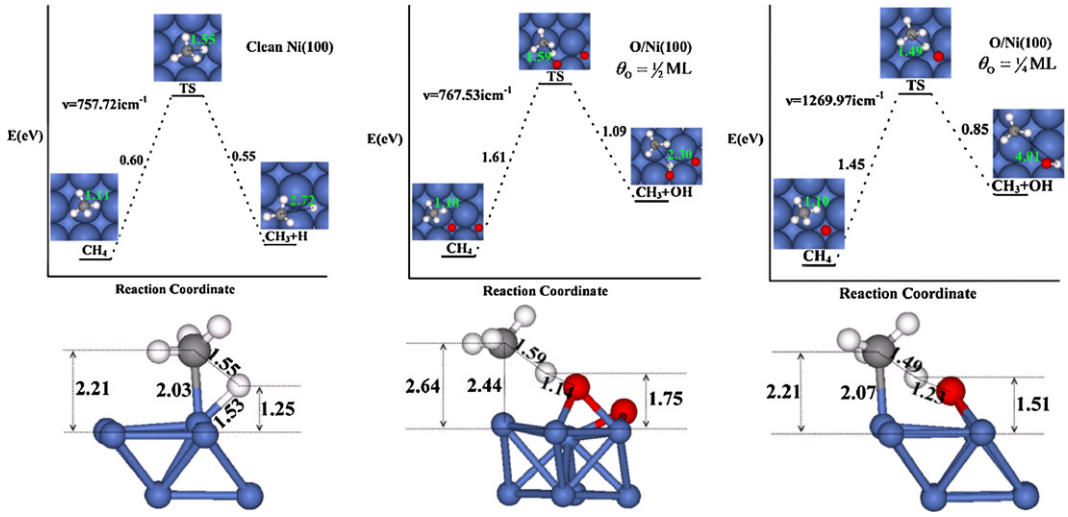


**Fig. 5.** Reaction energy profile of $CH_4$ dissociation and corresponding geometry parameter of TS on clean Ni(1 0 0) surface and O/Ni(1 0 0) surface with $\theta_O$ = 1/2 ML and $\theta_O$ = 1/4 ML. Bond lengths are in Å.

be $CH_3$(4h.) + H(4h.). The corresponding adsorption energy is −4.60 eV, while the adsorption energies of the other three systems are −4.47, −4.50 and −4.34 eV for bri/bri, top/bri and bri/4h., respectively (Table 4). Zhu et al. [1] calculated the energy of −4.74 to −4.28 eV for different co-adsorption sites. Lai et al. [3] obtained the energy of −2.10 to −1.85 eV relative to the H-covered surface and isolated $CH_3$. It can be seen from the result that the combination of the most stable adsorption site for isolated $CH_3$ (bridge site) and H (four-hold hollow site) is less stable than the others. This is because the initial distance between $CH_3$ and H is so close in such case as compared to other combinations, thus results in a large repulsion effect. The corresponding geometry parameters are shown in the illustration (Fig. 4a).

The activation barrier was calculated to be 0.60 eV, which is close to the experimental data gained by Nielsen et al. [6] (0.61 ± 0.02 eV). Lai et al. [3] proposed the activation barriers of 0.64 and 0.73 eV without and with spin-polarization. Zhu et al. [1] calculated the activation barrier of 0.61 eV and Swang et al. [17] reported the energy of 0.69 ± 0.04 eV. The reaction energy profile for $CH_4$ dissociation on Ni(1 0 0) surface and the corresponding geometry parameters of the transition state (TS) are shown in Fig. 5. During the reaction process, $CH_4$ molecule first approaches to the surface and the specified C–H bond starts to stretch. At the TS, the H fragment located close to the bridge site, while the $CH_3$ is near the top site. The C–H distance is 1.55 Å (compared with that of IS, 1.11 Å). The process is then completed by diffusion of these two fragments to the neighboring four-hold hollow sites.

### 3.2.2. O/Ni(1 0 0)

For the O/Ni(1 0 0) surfaces, the FS may appear as $CH_3$ + OH or $CH_3$ + H + O depending on the surface coverage of oxygen. At the lower oxygen coverage ($\theta_O$ = 1/6 and 1/9 ML), FS of $CH_3$ + OH or $CH_3$ + H + O are probably formed, however, only $CH_3$ + OH formed at high oxygen coverage. For the FS of

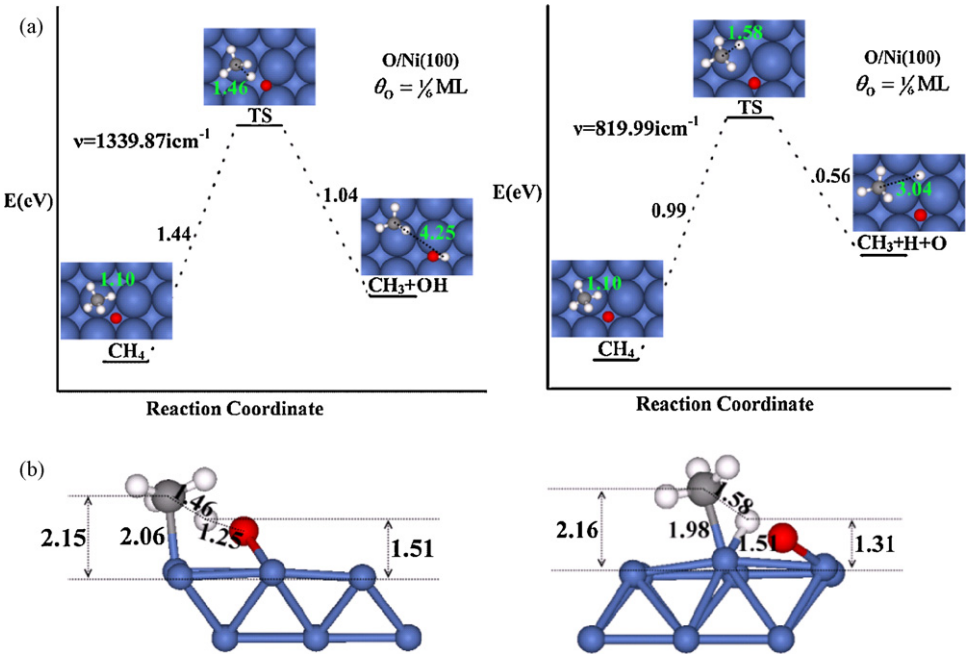


**Fig. 6.** Reaction energy profile of $CH_4$ dissociation and corresponding geometry parameters of TS on O/Ni(1 0 0) surface with $\theta_O$ = 1/6 ML. Bond lengths are in Å.

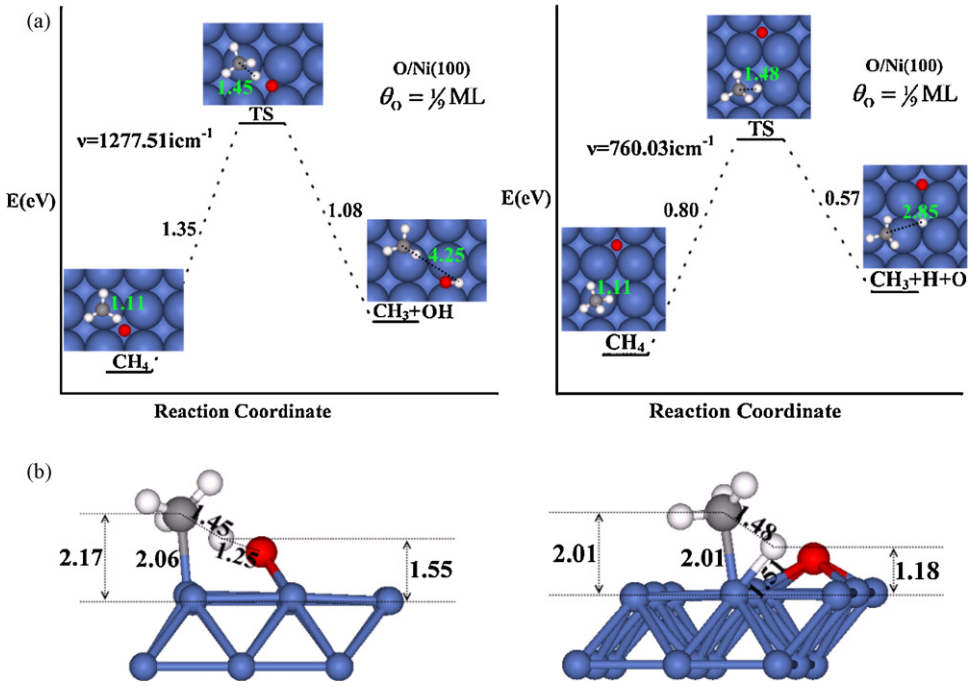


**Fig. 7.** Reaction energy profile of $CH_4$ dissociation and corresponding geometry parameters of TS on O/Ni(1 0 0) surface with $\theta_O$ = 1/9 ML. Bond lengths are in Å.

$CH_3$ + OH, the stable co-adsorption sites for $CH_3$ + OH on the O/Ni(1 0 0) surface with $\theta_O$ = 1/4 ML was firstly confirmed. Three co-adsorption sites, including $CH_3$(bri.) + OH(bri.), $CH_3$(top) + OH(bri.) and $CH_3$(bri.) + OH(4h.), were investigated. The most stable co-adsorption site is $CH_3$(bri.) + OH(bri.) with the corresponding co-adsorption energy of −4.22 eV. The calculated energy of the other two situations is −4.05 eV (top/bri) and −4.03 eV (bri/4h.), respectively. Based on this result, the co-adsorption sites on the other O/Ni(1 0 0) surfaces were studied. The co-adsorption energies of the most stable sites were calculated to be −4.24, −4.41 and −4.47 eV corresponding to different oxygen atom coverage ($\theta_O$ = 1/2, 1/6 and 1/9 ML). The related optimized equilibrium structures are given in Table 4 and Fig. 4b–e. For the FS of $CH_3$ + H + O, the oxygen atom is not involved in the reaction. The configurations of the most stable co-adsorption systems are very similar to that of clean Ni(1 0 0) surface except the $CH_3$ fragment is closer to the bridge site. The calculated co-adsorption energies are −4.27 and −4.38 eV for the oxygen coverage of 1/6 and 1/9 ML, respectively (the corresponding geometry parameters are shown in Fig. 4f and g).

According to the different FS, there are two different reaction mechanisms for $CH_4$ dissociation on O/Ni(1 0 0): $CH_4 + O \rightarrow CH_3 + OH$ and $CH_4 + O \rightarrow CH_3 + H + O$. For the former reaction mechanism, the calculated activation barriers are 1.61, 1.45, 1.44 and 1.35 eV for the cases of $\theta_O$ = 1/2, 1/4, 1/6 and 1/9 ML, respectively. As the similarity of the ISs and FSs, the reaction paths are basically the same. The beginning step is also the stretch of specified C–H bond of $CH_4$ molecule. At the TS, the H fragment is at the middle of $CH_3$ fragment and oxygen atom, while the $CH_3$ is near the top site and oxygen atom locates between four-hold site and bridge site. Specially, the H atom is not bound to surface Ni atom, which is different from that of clean Ni(1 0 0) surface. The subsequence process is the H fragment moves close to the oxygen atom. Then it is completed with the formation of hydroxyl and diffuses to the bridge site. The dissociating C–H bond lengths at different TSs are 1.59, 1.49, 1.46 and 1.45 Å. Figs. 5–7 show the reaction energy profiles for $CH_4$ dissociation and the geometry details of the TS corresponding to $\theta_O$ = 1/2, 1/4, 1/6 and 1/9 ML.

For the reaction mechanism of $CH_4 + O \rightarrow CH_3 + H + O$ with a lower coverage of O atom ($\theta_O$ = 1/6 and 1/9 ML), the corresponding activation barriers are 0.99 and 0.80 eV (Figs. 6 and 7). The whole process of the reaction is similar to that on the clean Ni(1 0 0) surface except for some differences in the TS. At the TS of O/Ni(1 0 0) with $\theta_O$ = 1/6 ML, the H fragment is located between the top site and four-hold site, while the $CH_3$ is near the top site. Then the process is completed by the diffusion of these two fragments to the most stable co-adsorption sites. For the TS of O/Ni(1 0 0) surface with $\theta_O$ = 1/9 ML, however, the H fragment is located close to the bridge site whereas the $CH_3$ is almost located to the top site, which is very similar to that of clean Ni(1 0 0).

### 3.2.3. NiO(1 0 0)

On NiO(1 0 0), four different co-adsorption sites, including $CH_3$ at Ni-top, bridge, or hollow site with H atom at the O-top site, were studied. The co-adsorption site of $CH_3$(Ni-top) + H(O-top) was found to be the most stable system with the adsorption energy of −4.85 eV. Fig. 4h illustrates the corresponding geometry structure of $CH_3$(Ni-top) + H(O-top). The activation barrier was calculated to be 1.64 eV, which is close to the activation barrier calculated by Hwang et al. [18] (1.23 eV). This kind of dissociation process is a little different from the former because oxygen atoms in this system are lattice oxygen atoms, which are not as free as pre-adsorbed oxygen atoms. At the TS, the H fragment is located at the bridge site. The $CH_3$ fragment is at the Ni-top site and the C atom is bound to surface Ni atom with C–Ni bond length of 2.06 Å. The C–H distance is 1.59 Å and the O–H distance is 1.20 Å. Then the H fragment moves to the O-top site and form hydroxyl with lattice oxygen atom. Fig. 8 shows the reaction energy profile and TS structure for $CH_4$ dissociation on the NiO(1 0 0) surface.

From the calculated activation barriers listed above, we know that the activation barrier for the dissociation of methane on clean Ni(1 0 0) is much lower than the value on the oxygen atom pre-covered Ni(1 0 0) and the NiO(1 0 0), it is thus identified that the activate site for $CH_4$ dissociation is the metallic Ni instead of the oxidized Ni. This is also in agreement with the experiential observations that the $CH_4$ easily dissociates into $CH_x$ and H on a metallic

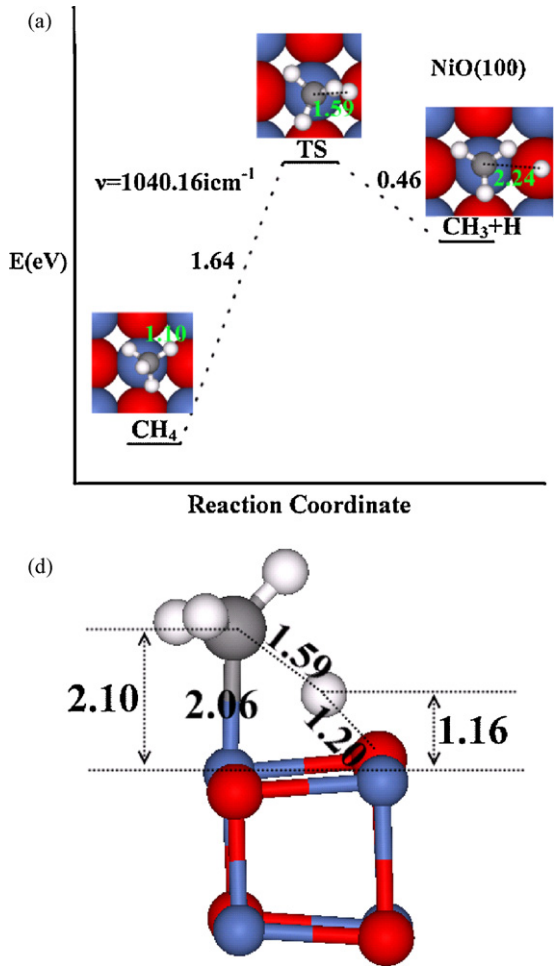


**Fig. 8.** Reaction energy profile of $CH_4$ dissociation and corresponding geometry parameters on NiO(1 0 0) surface. Bond lengths are in Å.

Ni catalyst instead of the oxidized catalyst [14] as well as NiO films [15].

### 3.3. Analysis of inhibition of methane dissociation by the presence of oxygen atom

Why and how the presence of oxygen atom inhibits the dissociation of methane? To answer this question, we intend to analyze from two aspects: one is the change of adsorption energy induced by the presence of oxygen, one is TS energy change affected by the oxygen atom.

#### 3.3.1. Adsorption energies review of possible species on different surfaces

From the calculated adsorption energies, it can be clearly seen that the adsorption properties of methane are similar on different surfaces. It prefers the Ni-top site and the configuration is basically the same as it is in the gas phase. So the pre-adsorbed oxygen atom does not have a strong effect on the initial state. The adsorption energies of $CH_3$ and H species on the O/Ni(1 0 0) surfaces and the NiO(1 0 0) surface are smaller than that on the clean Ni(1 0 0) surface. Here, $CH_3$ adsorption on the O/Ni(1 0 0) surface at the Ni-top site was chosen as an example to compare the effect of pre-adsorbed oxygen atom. As seen from Table 2, the adsorption energy of $CH_3$ is monotonously increasing with the decreasing of oxygen atom coverage. In addition, it can be seen from Table 2 that the adsorption energies of $CH_3$ on the O/Ni(1 0 0) surfaces under the conditions of the lower oxygen coverage ($\theta_O$ = 1/6 and 1/9 ML) are close to that of the clean Ni(1 0 0), as the surface conditions are similar.

Based on the previous results, the adsorption energy of species decreases in the presence of oxygen atom, and the possible reason will be analyzed by means of electronic structure discussion.

*3.3.1.1. Work function change.* Surface work function ($\Phi$) is the minimum energy required to eject an electron into vacuum at 0 K and it reflects the stability of surface electrons: larger values of work function corresponding to more stable electrons. $\Phi$ is calculated by the energy difference between the Fermi level ($E_{Fermi}$) and the vacuum level ($E_{Vacuum}$), $\Phi = E_{Vaccum} - E_{Fermi}$. Here $E_{Vaccum}$ is taken as the planar average if the potential. The work function of the clean Ni(1 0 0) surface was calculated to be 4.97 eV, and it agrees well with earlier theoretical results of 4.97 eV obtained by Kresse and Hafner [40] and Mittendorfer et al. [41]. For the O/Ni(1 0 0) surface, adsorption of oxygen atom leads to a surface electric dipole layer between it and the surface, which causes the change of work function. Since the electronegativities of oxygen (3.44) atom are greater than that of Ni (1.90) [42], the direction of the induced dipole moment is from oxygen to Ni(1 0 0). In our calculation, the work function is monotonously decreasing with the decline of pre-adsorbed oxygen atom coverage. The corresponding values are 5.66, 5.39, 5.06 and 5.03 eV. Yamagishi et al. [43] found the change of work function was 0.72 eV when oxygen atom adsorbed on Ni(1 1 1) ($\sqrt{3} \times \sqrt{3}$) R30° surface using first-principles DFT. The increase of work function after oxygen atom covered means the surface electron is attracted by oxygen atom and lead to a decrease of charge density around Fermi level, i.e. the adsorption energies of adsorbates are smaller. The adsorption energies of $CH_3$ at the same site (Ni-top site) on different surfaces are in consistent with the change of surface work function (Table 2). For the clean NiO(1 0 0) surface, the work function is 4.35 eV, which is in good agreement with other theoretical results (4.40 eV) [44] as well as the experimental observation (4.40 eV) [45]. Oxide system may induce significant changes in the work function of the metal support. The presence of the oxygen atoms reduces the amount of electronic charge that spills over from the metal surface, the metal electrons are polarized towards the surface, and the work function decreases compared with that of clean Ni(1 0 0) surface.

*3.3.1.2. Projected density of state analysis.* The d-band center is an important parameter to measure the distribution of solid energy levels and it characterizes the ability to eject an electron to the adsorbed molecule from the d-band of metal. The d-band center is calculated by the formula:

$$\varepsilon_d^c = \frac{\int_{-\infty}^{E_f} E\rho_d(E)\,dE}{\int_{-\infty}^{E_f} \rho_d(E)\,dE},$$

where $\rho_d$ represents the density of states projected onto Ni atom d band and $E_f$ is the Fermi energy. The d-band position has been widely used as one of the relevant measure for charactering kinds of metals by many researchers, e.g. Hammer and Nørskov [46] and Mavrikakis et al. [47]. Fig. 9 displays the projected density of state (PDOS) plot of metallic Ni d-band for different surfaces, clean Ni(1 0 0) surface, O/Ni(1 0 0) surfaces with different oxygen atom coverage. As seen from Fig. 9, the d-band centers are −2.47, −2.09, −2.02 and −1.90 eV corresponding to $\theta_O$ = 1/2, 1/4, 1/6 and 1/9 ML, respectively. This is in good agreement with the adsorption energies of $CH_3$ at Ni-top site on the O/Ni(1 0 0) surfaces with different oxygen atom coverage. Observably, the trend of d-band center change for O/Ni(1 0 0) surfaces is similar to that of work function change. The higher oxygen atom coverage, the further away it is from the Fermi level.

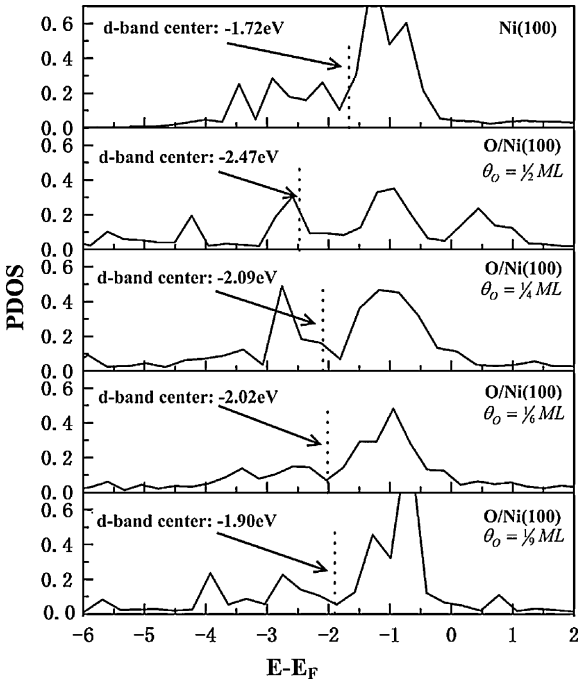


**Fig. 9.** Projected density of state (PDOS) onto d-band of Ni atom.

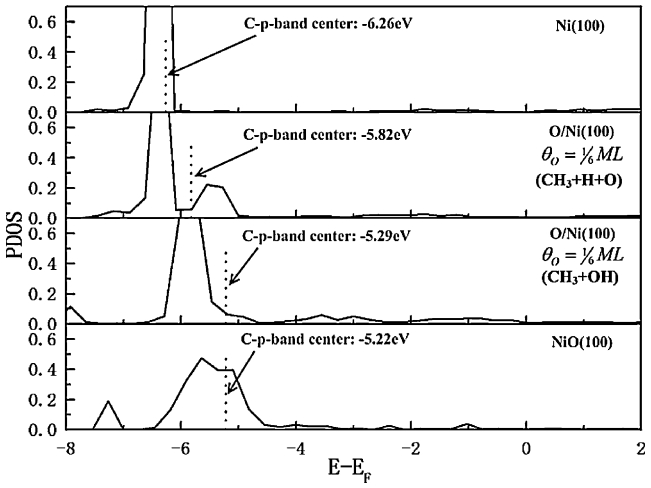


**Fig. 10.** Projected density of state (PDOS) onto C(p)-band in $CH_3$.

To further explore the possible reason for activation barrier change as a result of the presence of oxygen, the analysis of activation barrier is necessary.

### 3.3.2. Analysis of activation barrier

From the definition of $E_a$, we know that activation barrier is the difference between calculated total energy of IS and TS. From the calculated energy data listed in Table 1, one can see that the presence of oxygen atom has a little effect on the IS. So the influence of oxygen atom mainly reflects in the TS complex, and we will analyze in the following two aspects.

*3.3.2.1. Energy decomposition of activation barrier.* Because the two fragments at the TS are separated, so the activation barrier can be decomposed by the following form: $E_a = E^{gas}_{bond} - E^{IS}_{CH_4} + E^{TS}_{CH_3} + E^{TS}_{H} + E^{TS}_{int}$ [48]. This equation suggests that the activation barrier consists of three parts: (i) $E^{gas}_{bond}$, the bonding energy of methane in the gas phase; (ii) $E^{IS}_{CH_4}$, $E^{TS}_{CH_3}$ and $E^{TS}_{H}$, the adsorption energies of individual species in the IS and TS; and (iii) $E^{TS}_{int}$, the interaction energy between $CH_3$ and H in the TS, which is believed to consist of two parts [49–52]: (i) the *direct Pauli repulsion* between $CH_3$ and H, which is strongly dependent on the distance between them; and (ii) the *bonding competition effect* caused by sharing substrate atoms between $CH_3$ and H, which is related to the height over surface of these two groups.

Three typical models were investigated, namely, the clean Ni(1 0 0) surface, the O/Ni(1 0 0) surface ($\theta_O$ = 1/6 ML), and the NiO(1 0 0) surface. From our calculated energy results as listed in Table 5, it can be found that if oxygen atom involves in the reaction, via forming the O–H bond, the repulsion effect between $CH_3$ and H in TS is smaller than that of the clean Ni(1 0 0) (0.54 vs. 0.12 eV as seen in Table 5). If not, the interaction energies are basically the same as the clean Ni(1 0 0) (0.54 vs. 0.41 eV). Moreover, from the adsorption energies of $CH_3$ and H in the TS, it can be found that the pre-adsorbed oxygen atom and the lattice oxygen atoms both weaken the adsorption of $CH_3$ and H in the TS (by 0.11–0.50 eV in the former case and 0.35–0.99 eV in the latter case, respectively), which greatly increases the activation barrier. From the TS configuration shown in Figs. 5, 6 and 8, one can see distinctive difference between different reaction mechanism: the H fragment is not bound to the surface Ni atom if the oxygen atom involves in the reaction, and the H atom is bound to the surface Ni atom and form a three-center bond (like H–Ni–C type) [53] that would stabilize the TS when the oxygen atom just as a spectator. So the latter situations have more stable TS than the former ones due to the formation of three-center bond. The overall result is that the oxidized Ni has higher activation barrier than that of metallic Ni, i.e. the existence of oxygen atom inhibits the dissociation of methane catalyzed by Ni.

*3.3.2.2. Projected density of state analysis of $CH_3$ fragment in the TS.* From the energy decomposition analysis of the TS, it can be seen that the pre-adsorbed oxygen atom weakens the adsorption of $CH_3$ in the TS. The analysis of the PDOS on the p orbital of C atom can be helpful to get a further understanding of the interaction between $CH_3$ and surface. As seen in Fig. 10, the atomic carbon p-band centers are −6.26, −5.82, −5.29 and −5.22 eV for the clean Ni(1 0 0), O/Ni(1 0 0) ($\theta_O$ = 1/6 ML with two different reaction paths)

**Table 5**
Energy decomposition of the calculated activation barrier.

| | $E^{IS}_{CH_4}$ (eV) | $E^{TS}_{CH_3}$ (eV) | $E^{TS}_{H}$ (eV) | $E^{TS}_{int}$ (eV) | $E_a$ (eV) |
|---|---|---|---|---|---|
| Ni(1 0 0) | 0.10 | −2.03 | −2.65 | 0.54 | 0.60 |
| O/Ni(1 0 0) ($\theta_O$ = 1/6 ML) | | | | | |
| $CH_3$ + OH | 0.04 | −1.55 (0.48) | −1.93 (0.72) | 0.12 (−0.42) | 1.44 |
| $CH_3$ + H + O | 0.04 | −1.92 (0.11) | −2.30 (0.35) | 0.41 (−0.13) | 0.99 |
| NiO(1 0 0) | −0.06 | −1.53 (0.50) | −1.66 (0.99) | −0.07 (−0.61) | 1.64 |

*Note*: $\sum E = E^{TS}_{CH_3} + E^{TS}_{H}$. Here, the C–H bonding energy of $CH_4$ ($E^{gas}_{bond}$) is calculated to be 4.84 eV. The data in the parentheses indicate the different component's contribution (increase or decrease) to the activation barrier compared to clean Ni(1 0 0) surface.

and NiO(1 0 0) surface, respectively. The shift of the peak towards the lower energy is larger for clean Ni(1 0 0) surface than that of the other cases, which is consistent with the largest $CH_3$ adsorption energy in the TS among these studied models.

## 4. Conclusions

In this work, the slab model was used to investigate the adsorption and dissociation of methane catalyzed by Ni with DFT calculation. Also the effect of the oxygen atom pre-adsorbed on the surface with different coverage ($\theta_O$ = 1/2, 1/4, 1/6 and 1/9 ML) is considered. On the clean Ni(1 0 0), the activation energy for the methane dissociation is found to be 0.60 eV. The calculated activation barrier of O/Ni(1 0 0) surface is monotonously decreasing with the reducing of the pre-adsorbed oxygen atom coverage. The corresponding values are 1.61, 1.45, 1.44 and 1.35 eV. The activation barrier of methane dissociation on NiO(1 0 0) surface is 1.64 eV, which is close to that on the O/Ni(1 0 0) ($\theta_O$ = 1/2 ML). The result indicates that the presence of oxygen atom inhibits the dissociation of methane both kinetically and thermodynamically. Moreover, the decomposition of activation barrier provides a further understanding of how the existence of oxygen atom increases the barrier. It is found that though the pre-adsorbed oxygen atom decreases the interaction between $CH_3$ and H in the transition state, it *greatly decreases the interaction of $CH_3$ and H with substrate*, so the overall result is that the presence of oxygen atom inhibits the dissociation of methane on Ni surface.

## Acknowledgments

This work was supported by the National Natural Science Foundation of China (Grants Nos. 20273034 and 20673063) and the NKStar HPC program.

## References

[1] Y.A. Zhu, Y.C. Dai, D. Chen, W.K. Yuan, J. Mol. Catal. A: Chem. 264 (2007) 299.
[2] J.R. Rostrup-Nielsen, in: J.R. Anderson, M. Boudart (Eds.), Catalysis, Science and Technology, vol. 5, Springer, Berlin, 1984, p. 1.
[3] W.Z. Lai, D.Q. Xie, D.H. Zhang, Surf. Sci. 594 (2005) 83.
[4] T.P. Beebe Jr., D.W. Goodman, B.D. Kay, J.T. Yates Jr., J. Chem. Phys. 87 (1987) 2305.
[5] I. Chorkendorff, I. Alstrup, S. Ullmann, Surf. Sci. 227 (1990) 291.
[6] B.O. Nielsen, A.C. Luntz, P.M. Holmblad, I. Chorkendorff, Catal. Lett. 32 (1995) 15.
[7] R.C. Egeberg, S. Ullmann, I. Alstrup, C.B. Mullins, I. Chorkendorff, Surf. Sci. 497 (2002) 183.
[8] H.S. Bengaard, I. Alstrup, I. Chorkendorff, S. Ullmann, J.R. Rostrup-Nielsen, J.K. Nørskov, J. Catal. 187 (1999) 238.
[9] R.D. Beck, P. Maroni, D.C. Papageorgopoulos, T.T. Dang, M.P. Schmid, T.R. Rizzo, Science 187 (1999) 238.
[10] P.M. Holmblad, J. Wambach, I. Chorkendorff, J. Chem. Phys. 102 (1995) 8255.
[11] L.B.F. Juurlink, P.R. McCabe, R.R. Smith, C.L. DiCologero, A.L. Utz, Phys. Rev. Lett. 83 (1999) 868.
[12] M.P. Schmid, P. Maroni, R.D. Beck, T.R. Rizzo, J. Chem. Phys. 117 (2002) 8603.
[13] Y.H. Hu, E. Ruckenstein, Adv. Catal. 48 (2004) 297.
[14] Y.H. Hu, E. Ruckenstein, J. Phys. Chem. A 102 (1998) 10568.
[15] R.A. Campbell, J. Szanyi, P. Lenz, D.W. Goodman, Catal. Lett. 17 (1993) 39.
[16] H. Burghgraef, A.P.J. Jansen, R.A. van Santen, J. Chem. Phys. 101 (1994) 11012.
[17] O. Swang, K. Faegri Jr., O. Gropen, U. Wahlgren, P. Siegbahn, Chem. Phys. 156 (1991) 379.
[18] D.Y. Hwang, A.M. Mebel, J. Phys. Chem. A 106 (2002) 12072.
[19] G. Kresse, J. Furthmüller, Comput. Mater. Sci. 6 (1996) 15.
[20] G. Kresse, J. Furthmüller, Phys. Rev. B 54 (1996) 11169.
[21] Y. Morikawa, K. Iwata, K. Terakura, Appl. Surf. Sci. 169–170 (2001) 11.
[22] G. Kresse, J. Hafner, Phys. Rev. B 47 (1993) 558.
[23] P.E. Blöchl, Phys. Rev. B: Condens. 59 (1994) 17953.
[24] G. Kresse, D. Joubert, Phys. Rev. B 59 (1999) 1758.
[25] G. Mills, H. Jónsson, Phys. Rev. Lett. 72 (1994) 1124.
[26] G. Mills, H. Jónsson, G.K. Schenter, Surf. Sci. 324 (1995) 305.
[27] G. Henkelman, B.P. Uberuaga, H. Jónsson, J. Chem. Phys. 113 (2000) 9901.
[28] H.J. Monkhorst, J.D. Pack, Phys. Rev. B 13 (1976) 5188.
[29] A.A. Phatak, W.N. Delgass, F.H. Ribeiro, W.F. Schneider, J. Phys. Chem. C 113 (2009) 7269.
[30] C. Oliva, C. van den Berg, J.W. Niemantsverdriet, D. Curulla-Ferré, J. Catal. 245 (2007) 436.
[31] C. Kittel, Introduction to Solid State Physics, 7th ed., Wiley, New York, 1996.
[32] X.Y. Pang, L.Q. Xue, G.C. Wang, Langmuir 23 (2007) 4910.
[33] L.Q. Xue, X.Y. Pang, G.C. Wang, J. Phys. Chem. C 111 (2007) 2223.
[34] A. Goursot, F. Mele, N. Russo, D.R. Salahub, M. Toscano, Int. J. Quant. Chem. 48 (1993) 277.
[35] P.E.M. Siegbahn, U. Wahlgren, Int. J. Quant. Chem. 42 (1992) 1149.
[36] S.E. Wonchoba, D.G. Truhlar, J. Phys. Chem. B 102 (1998) 6842.
[37] P.E.M. Siegbahn, I. Panas, Surf. Sci. 240 (1990) 37.
[38] T.H. Upton, J. Vac. Sci. Technol. 20 (1982) 527.
[39] K. Christmann, R.J. Behm, G. Ertl, J. Chem. Phys. 70 (1979) 4168.
[40] G. Kresse, J. Hafner, Surf. Sci. 459 (2000) 287.
[41] F. Mittendorfer, A. Eichler, J. Hafner, Surf. Sci. 423 (1999) 1.
[42] D.R. Lide, CRC Handbook of Chemistry and Physics, Section 9, Molecular Structure and Spectroscopy, Electronegativity, 84th ed., CRC Press, 2003–2004.
[43] S. Yamagishi, S.J. Jenkins, D.A. King, Surf. Sci. 543 (2003) 12.
[44] N. Yu, W.B. Zhang, N. Wang, Y.F. Wang, B.Y. Tang, J. Phys. Chem. C 112 (2008) 452.
[45] R. Reissner, M. Schulze, Surf. Sci. 454–456 (2000) 183.
[46] B. Hammer, J.K. Nørskov, Surf. Sci. 343 (1995) 211.
[47] M. Mavrikakis, B. Hammer, J.K. Nørskov, Phys. Rev. Lett. 81 (1998) 2819.
[48] Z.P. Liu, P. Hu, J. Am. Chem. Soc. 125 (2003) 1958.
[49] Z.P. Liu, P. Hu, J. Chem. Phys. 114 (2001) 8244.
[50] J.J. Mortensen, B. Hammer, J.K. Nørskov, Surf. Sci. 414 (1998) 315.
[51] A. Alavi, P. Hu, T. Deutsch, P.L. Silvestrelli, J. Hutter, Phys. Rev. Lett. 80 (1998) 3650.
[52] K. Bleakley, P. Hu, J. Am. Chem. Soc. 121 (1999) 7644.
[53] C.J. Zhang, P. Hu, J. Chem. Phys. 116 (2002) 322.